Inorg. Chem. **2006**, *45*, 11035–11042

Concerning the Electronic Coupling of MoMo Quadruple Bonds Linked by 4,4′-Azodibenzoate and Comparison with t_{2g}^6-Ru(II) Centers by 4,4′-Azodiphenylcyanamido Ligands

Malcolm H. Chisholm,* Jason S. D'Acchioli, Christopher M. Hadad,* and Nathan J. Patmore

Department of Chemistry, The Ohio State University, 100 West 18th Avenue, Columbus, OH 43210-1185

Received May 31, 2006

From the reactions between $Mo_2(O_2C^tBu)_4$ and each of terephthalic acid and 4,4′-azodibenzoic acid, the compounds $[Mo_2(O_2C^tBu)_3]_2(\mu\text{-}O_2CC_6H_4CO_2)$ (**1**) and $[Mo_2(O_2C^tBu)_3]_2(\mu\text{-}O_2CC_6H_4N_2C_6H_4CO_2)$ (**2**) have been made and characterized by spectroscopic and electrochemical methods. Their electronic structures have been examined by computations employing density functional theory on model compounds where HCO_2 substitutes for $^tBuCO_2$. On the basis of these studies, the two Mo_2 units are shown to be only weakly coupled and the mixed-valence ions $\mathbf{1}^+$ and $\mathbf{2}^+$ to be valence-trapped and Class II and I, respectively, on the Robin–Day classification scheme for mixed-valence compounds. These results are compared to t_{2g}^6-Ru centers linked by 1,4-dicyanamidobenzene and azo-4,4′-diphenylcyanamido bridges for which the mixed-valence ions $[Ru–bridge–Ru]^{5+}$ have been previously classified as fully delocalized, Class III [Crutchley et al. *Inorg. Chem.* **2001,** *40*, 1189; *Inorg. Chem.* **2004,** *43*, 1770], and on the basis of results described herein, it is proposed that the latter complex ion is more likely a mixed-valence organic radical where the bridge is oxidized and not the Ru(2+) centers.

Introduction

Electron transfer and electron delocalization via a bridge connecting two redox-active metal centers are closely related phenomena that permeate numerous chemical, physical, and biological systems.[1−5] The study of the interaction of two redox-active and otherwise equivalent metal centers separated by a bridge has a history in inorganic chemistry spanning the past four decades. Prominent among these studies were those involving the Creutz−Taube ion $[(NH_3)_5Ru\text{-}pz\text{-}Ru(NH_3)_5]^{5+}$. Although prepared in 1968,[6] the Creutz−Taube ion was not recognized as an example of a fully delocalized compound (Class III)[7] until 1991.[8,9] It is fair to state that the Creutz−Taube ion inspired and attracted numerous chemists to this field of study. Of the many mixed-valence complexes in well-defined coordination environments, the Ru^{II}−bridge−Ru^{III} and related t_{2g}^6−bridge−t_{2g}^5 systems have remained the object of significant attention.[8,10,11] Compounds close to the Class II/III border, which is crossed on going from strongly coupled to fully delocalized, are still a major focus of current research.[2,12,13]

From all of this work, two general principles pertaining to the electronic coupling of two redox-active centers, be they inorganic metal centers or organic radicals, become evident: (1) as the distance of the bridge increases, the electronic coupling decreases[14,15] and (2) for a two-state model, the electronic coupling is a measure of the sum of electron transfer and hole transfer through the bridge.[16,17] In

* To whom correspondence should be addressed.

(1) Beratan, D. N.; Onuchic, J. N.; Winkler, J. R.; Gray, H. B. *Science* **1992**, *258*, 1740.
(2) Demadis, K. D.; Hartshorn, C. M.; Meyer, T. J. *Chem. Rev.* **2001**, *101*, 2655.
(3) Huynh, M. H. V.; Dattelbaum, D. M.; Meyer, T. J. *Coord. Chem. Rev.* **2005**, *249*, 457.
(4) Joachim, C.; Ratner, M. A. *Nanotechnology* **2004**, *15*, 1065.
(5) Lewis, F. D.; Letsinger, R. L.; Wasielewski, M. R. *Acc. Chem. Res.* **2001**, *34*, 159.
(6) Creutz, C.; Taube, H. *J. Am. Chem. Soc.* **1968**, *91*, 3988.
(7) Robin, M. B.; Day, P. *Adv. Inorg. Radiochem.* **1967**, *10*, 247.
(8) Crutchley, R. J. *Adv. Inorg. Chem.* **1994**, *41*, 273.
(9) Oh, D. H.; Sano, M.; Boxer, S. G. *J. Am. Chem. Soc.* **1991**, *113*, 6880.
(10) Kaim, W. K.; Klein, A.; Glockle, M. *Acc. Chem. Res.* **2000**, *33*, 755.
(11) Launay, J.-P. *Chem. Soc. Rev.* **2001**, *30*, 386.
(12) Brunschwig, B. S.; Creutz, C.; Sutin, N. *Chem. Soc. Rev.* **2002**, *31*, 168.
(13) Nelson, S. F. *Chem. Eur. J.* **2000**, *6*, 581.
(14) Cotton, F. A.; Donahue, J. P.; Murillo, C. A. *J. Am. Chem. Soc.* **2003**, *125*, 5436.
(15) Xu, G.-L.; Zou, G.; Ni, Y.-H.; DeRosa, M. C.; Crutchley, R. J.; Ren, T. *J. Am. Chem. Soc.* **2003**, *125*, 10057.
(16) Creutz, C.; Newton, M. D.; Sutin, N. *J. Photochem. Photobiol. A: Chem.* **1994**, *82*, 47.

10.1021/ic060956w CCC: $33.50
Published on Web 12/05/2006

general, however, one situation dominates, either electron transfer or hole transfer.

Inspired by the work of Tour et al. on enhancing the electrical conductivity of polythiophenes by employing alternating donor−acceptor units in the chain,[18] Crutchley and co-workers prepared the 4,4′-azo-di-phenylcyanamido (μ-adpc)-bridged diruthenium compound [(trpy)(bpy)Ru]$_2$-(μ-adpc)(PF$_6$)$_2$ where trpy = 2,2′:6′,2″-terpyridine and bpy = 2,2′-bipyridine.[19,20] The mixed-valence analogue of this compound is depicted in (α) below. This compound is unique

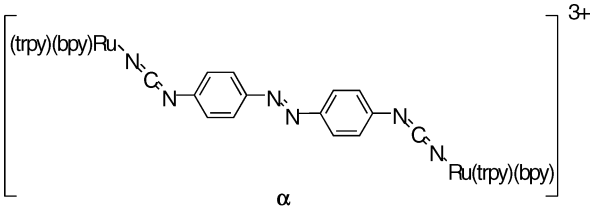

α

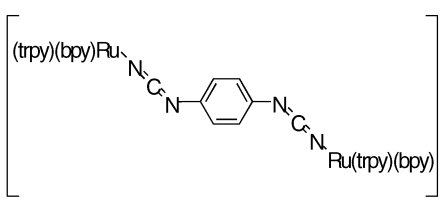

β

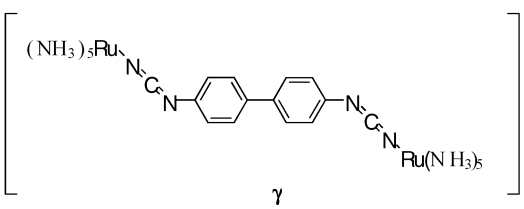

γ

among the whole family of Ru^{II}−bridge−Ru^{III} mixed-valence compounds, being classified as fully delocalized in its mixed-valence state for metal atoms separated by >10 Å. The magnitude of $K_c = 1.3 \times 10^{13}$, determined electrochemically from the separation of its first and second oxidation waves, can be compared with $K_c = 2.7 \times 10^7$ for the related μ-1,4-dicyanamidobenzene-bridged complex[21] (β) and the K_c = 16 observed for the weakly coupled mixed-valence ion [(NH$_3$)$_5$Ru]$_2$(μ-bp)$^{3+}$, where bp^{2-} = 4,4′-biphenyldicyanamide (γ).[22]

The adpc mixed-valence ion (α) also showed a strong ($\epsilon \approx 7000$ M^{-1} cm^{-1}) absorption in the near-IR at 1800 nm (5560 cm^{-1}) in acetonitrile solvent, which was assigned to the IVCT transition. For a Class III fully delocalized system, this gives H_{ab} = 2780 cm^{-1} which again is exceptionally large for two Ru centers separated by 19.5 Å.

Our own work in the area of electronic coupling between metal−metal (M$_2$) quadruply bonded units lead us to prepare and compare the properties of the Mo$_2$ quadruply bonded species linked by terephthalate, (O$_2$C−C$_6$H$_4$−CO$_2$)$^{2-}$, and 4,4′-azodibenzoate, (O$_2$C−C$_6$H$_4$−N=N−C$_6$H$_4$−CO$_2$)$^{2-}$ (adb^{2-}). The latter carboxylate contains the core C$_6$H$_4$−N=N−C$_6$H$_4$ of the adpc^{2-} unit, while the former can be viewed as the control complex where only a small degree of electronic coupling is expected.

Experimental Section

Synthetic Methods. All manipulations were performed under an inert atmosphere (argon or nitrogen) using Schlenk and drybox techniques. THF was dried via reflux over sodium/benzophenone; toluene and hexanes were dried by reflux over sodium metal. All solvents were then stored over 4 Å molecular sieves and vigorously degassed to remove oxygen. THF-d_8 was dried over sodium metal, degassed by freeze−pump−thawing, and stored over 4 Å molecular sieves. DMSO-d_6 was dried by storing over molecular sieves and degassed by freeze−pump−thawing. The starting material Mo$_2$(O$_2$C^{t}Bu)$_4$ was prepared according to literature methods.[23]

Cyclic voltammetry (CV) and differential pulse voltammetry (DPV) studies were performed with a Princeton Applied Research (PAR) Model 173A potentiostat−galvanostat equipped with a PAR 176 current-to-voltage converter. A standard three-electrode cell was utilized in a nitrogen-filled drybox. The working electrode was a 1 mm polyethylether ketone (PEEK) platinum electrode purchased from BAS, while platinum wire was utilized as the auxiliary electrode. A pseudo-reference electrode was freshly prepared prior to each experiment by placing a silver wire in either 0.05 M TBABArF$_{24}$/THF (TBA = [^{n}BuN]$_4$, BArF$_{24}$ = [B{C$_6$H$_3$(CF$_3$)$_2$}$_4$]; vide infra) or 0.05 TBAPF$_6$/THF solution. TBAPF$_6$ was purchased from Aldrich and used after four recrystallizations from hot ethanol or until scans of the electrolyte solution showed the absence of any impurity peaks in the potential window. Cyclic voltammograms were acquired at a scan rate of 500 mV s^{-1} while differential pulse voltammograms were acquired at 36 mV s^{-1}. All potential values were referenced to the FeCp$_2$/FeCp$_2^+$ couple, obtained by adding a small amount of ferrocene to the sample after each experiment.

UV−visible spectroscopic studies were performed using a Perkin-Elmer Lambda 19 UV−vis−NIR absorption spectrometer. Spectra were obtained using a quartz cell with a 1 mm path length modified for use with air-sensitive compounds. ^{1}H NMR spectra were recorded on either Bruker DPX-250 or DPX-400 spectrometers at 250 and 400 MHz, respectively.

Matrix-assisted laser desorption ionization (MALDI) mass spectra of all [M$_2$]$_2$ complexes were performed at OSU's Campus Chemical Instrument Center (CCIC) using a Bruker Reflex III MALDI-TOF spectrometer. Samples were mixed with a dithranol matrix to aid in the effective ionization of the molecules. All complexes were kept under an inert atmosphere. Electrospray ionization (ESI) was performed with a Micromass Q-TOF II mass spectrometer with an auto-injector. Samples were prepared in a 9:11 mixture of THF/methanol with NaI as an internal standard.

Synthesis of 4,4′-Azodibenzoic Acid. 4,4′-Azodibenzoic acid was synthesized according to a revised literature procedure.[24−26] A 500 mL round-bottom flask was charged with 7.0 g of

(17) Evans, C. E. B.; Naklicki, M. L.; Rezvani, A. R.; White, C. A.; Kondratiev, V. V.; Crutchley, R. J. *J. Am. Chem. Soc.* **1998**, *120*, 13096.
(18) Zhang, Q. T.; Tour, J. M. *J. Am. Chem. Soc.* **1998**, *120*, 5355.
(19) Al-Noaimi, M.; Yap, G. P. A.; Crutchley, R. J. *Inorg. Chem.* **2004**, *43*, 1770.
(20) Mosher, P. J.; Yap, G. P. A.; Crtuchley, R. J. *Inorg. Chem.* **2001**, *40*, 1189.
(21) Rezvani, A. R.; Evans, C. E. B.; Crutchley, R. J. *Inorg. Chem.* **1995**, *34*, 4600.
(22) Aquino, M. A. S.; White, C. A.; Bensimon, C.; Greedan, J. E.; Crutchley, R. J. *Can. J. Chem.* **1996**, *74*, 2201.
(23) Brignole, A. B.; Cotton, F. A. *Inorg. Synth.* **1971**, *13*, 81.
(24) Mukherjee, P. S.; Das, N.; Kryschenko, Y. K.; Arif, A. M.; Stang, P. J. *J. Am. Chem. Soc.* **2004**, *126*, 2464−2473.
(25) Reid, E. B.; Pritchett, E. G. *J. Org. Chem.* **1953**, *18*, 715−719.
(26) Tomlinson, M. L. *J. Chem. Soc. Perkin Trans. 1* **1946**, 756.

4-nitrobenzoic acid. Approximately 100 mL of a 400 M NaOH solution was added to the organic acid, and the round-bottom flask was heated to ca. 70 °C on a hot water bath. A separate 250 mL round-bottom flask was charged with 60 g of glucose, which was dissolved in 100 mL of water. The glucose solution was heated to ca. 70° to ensure complete dissolution. The glucose solution was then added slowly to the NaOH/4-nitrobenzoic acid mixture, whereupon a bright yellow precipitate formed. Further addition of the glucose solution resulted in the precipitate turning brown.

The resulting solution had a stream of oxygen drawn through it for 4 days. The precipitate was then filtered and washed with three 50 mL aliquots of cold water and dissolved in 300 mL of hot water. The solution was acidified with acetic acid, whereupon a pink solid precipitated. The crude organic acid was then purified by stirring in 158 mL of a 1.0 M ammonium hydroxide solution for at least 30 min, or until most of the solid had dissolved. The solution was filtered, and the remaining solid discarded. The mother liquor was acidified with acetic acid, and then enough concentrated HCl was added to make the solution 10% HCl by volume. The solid was filtered, and the purification process was repeated with the remaining solid. The purified acid was washed with three 50 mL aliquots of cold water, followed by three 50 mL aliquots of diethyl ether. The acid was dried in vacuo at ca. 80 °C. Yield: 2.45 g. Anal. Calcd for $C_{14}H_{10}O_4N_2$: C, 62.22; H, 3.73; N, 10.37. Found: C, 61.26; H, 3.72; N, 10.05. ^{1}H NMR (DMSO-d_6, 250 MHz): δ 8.13 (d, 4H$_{AX}$, ^3J = 8.43 Hz), 7.97 (d, 4H$_{AX}$, ^3J = 8.43 Hz) ppm. ESI-TOF: Calculated monoisotopic MW: 270.26 (M^+). Found: 270.06 *m*/*z*.

Synthesis of [(^{t}BuCO$_2$)$_3$Mo$_2$]$_2$(μ-O$_2$CC$_6$H$_4$CO$_2$), 1. This compound was prepared in an analogous manner to [(^{t}BuCO$_2$)$_3$Mo$_2$]$_2$(μ-adb) from Mo$_2$(O$_2$C^{t}Bu)$_4$ (0.800 g, 1.34 mmol) and terephthalic acid (0.111 g, 0.668 mmol). An orange powder was isolated via centrifugation. The powder was washed six times with ca. 30 mL of toluene, and three times with ca. 30 mL of hexanes. The complex was dried in vacuo at 80 °C and isolated as an orange powder. Yield: 0.699 g (91%) Anal. Calcd for $C_{38}H_{58}O_{16}Mo_4$: C, 39.53; H, 5.06. Found: C, 37.91; H, 4.97. ^{1}H NMR (THF-d_8, 400 MHz): δ 8.34 (s, 4H), δ 1.43 (s, 18H), δ 1.39 (s, 36H) ppm. MALDI-TOF: Calculated monoisotopic MW: 1154.62 (M^+). Found: 1153.00 *m*/*z*. The low carbon count in the elemental analysis is accounted for by the presence of higher-order oligomers. This was verified by MALDI-TOF mass spectrometry, which revealed the presence of small quantities of bridged chains.

Synthesis of [(^{t}BuCO$_2$)$_3$Mo$_2$]$_2$(μ-adb), 2. A 50 mL Schlenk tube was charged with 4,4′-azodibenzoic acid (0.146 g, 0.538 mmol) and Mo$_2$(O$_2$C^{t}Bu)$_4$ (0.701 g, 1.18 mmol). Toluene (ca. 20 mL) was added, and the solution was stirred for 14 days, during which time it became dark blue in color. The product was isolated as a powder via centrifugation and washed six times with ca. 30 mL of toluene and three times with 30 mL of hexanes. The product was dried in vacuo at ca. 80 °C. Repeated attempts to grow crystals suitable for X-ray diffraction were unsuccessful. Yield: 0.312 g (46%). Anal. Calcd for $C_{44}H_{62}O_{16}N_2Mo_4$: C, 41.78; H, 5.42; N, 2.21. Found: C, 41.42; H, 4.88; N, 2.42. ^{1}H NMR (THF-d_8, 250 MHz): δ 8.29 (d, 4H$_{AX}$, ^3J = 8.5 Hz), 8.29 (d, 4H$_{AX}$, ^3J = 8.5 Hz), 1.44 (s, 18H), 1.39 (s, 36H) ppm. MALDI-TOF: Calculated monoisotopic MW: 1258.80 (M^+). Found: 1258.40 *m*/*z*.

Synthesis of ^{n}Bu$_4$N[B{C$_6$H$_3$(CF$_3$)$_2$}$_4$] (TBABArF$_{24}$) Supporting Electrolyte. Na[B{C$_6$H$_3$(CF$_3$)$_2$}$_4$] was synthesized according to literature methods.[27,28] TBABArF$_{24}$ was synthesized via the metathesis of Na[B{C$_6$H$_3$(CF$_3$)$_2$}$_4$] and [^{n}Bu$_4$N][Cl]. The complex was recrystallized at least five times by dissolving in ca. 1−2 mL of CH_2Cl_2 and adding ca. 1−2 mL of pentanes. The solution was placed in a freezer for 24 h, and the solid was filtered, washed three times with ca. 30 mL of pentanes, and dried in vacuo. Purity was gauged by the compound's appearance (snow white), as well as the absence of any impurity peaks in the CV spectral window.

Computational Details. Electronic structure calculations were performed using density functional theory (DFT) as implemented in the Gaussian 03 suite of programs.[29] The B3LYP exchange−correlation functional[29−32] along with the 6-31G* basis set[33] (with 5d functions) was used for H, C, O, and N, along with the SDD energy-consistent pseudopotential for Ru and Mo.[34] Geometry optimizations on the formate model complexes [(HCO$_2$)$_3$Mo$_2$]$_2$(μ-adb) and [(HCO$_2$)$_3$Mo$_2$]$_2$(μ-O$_2$CC$_6$H$_4$CO$_2$) were performed under C_{2h} and D_{2h} symmetry, respectively. The free ligand adpc^{2-} was geometry-optimized in C_{2h} symmetry. All complexes were found to be minima on their respective potential energy surfaces through vibrational frequency analyses. Electronic absorption spectra were predicted using the time-dependent density functional theory (TD-DFT) method as implemented within Gaussian 03 using the default optimization criteria.[35−37] All geometry-optimized coordinates are given in the Supporting Information. A single-point energy calculation with tight SCF convergence criteria was performed for [(trpy)(bpy)Ru]$_2$(μ-adpc)$^{2+}$ in C_i symmetry (the crystal structure has a crystallographically imposed center of inversion) using the reported crystal structure geometry. Orbital diagrams were generated using GaussView.[38]

Results and Discussion

Compounds **1** and **2** (Scheme 1) were prepared from the reactions between Mo$_2$(O$_2$C^{t}Bu)$_4$ and terephthalic and 4,4′-azo-dibenzoic acid, respectively, as shown in eq 1.

$$2\mathrm{Mo_2(O_2C^tBu)_4} + \mathrm{HO_2C{-}R{-}CO_2H} \xrightarrow[\sim 7\ \mathrm{days}]{\mathrm{toluene}} [(^t\mathrm{BuCO_2})_3\mathrm{Mo_2}]_2(\mu\text{-}\mathrm{O_2C{-}R{-}CO_2}) \quad (1)$$

In the solid state, **1** is orange while **2** is purple. Both compounds are air-sensitive, sparingly soluble in toluene,

(27) Reger, D. L.; Wright, T. D.; Little, C. A.; Lamba, J. J. S.; Smith, M. D. *Inorg. Chem.* **2001**, *40*, 3810−3814.
(28) Tellers, D. M.; Yung, C. M.; Arndtsen, B. A.; Adamson, D. R.; Bergman, R. G. *J. Am. Chem. Soc.* **2002**, *124*, 1400−1410.
(29) Frisch, M. J.; Trucks, G. W.; Schlegel, H. B.; Scuseria, G. E.; Robb, M. A.; Cheeseman, J. R.; Montgomery, J. A., Jr.; Vreven, T.; Kudin, K. N.; Burant, J. C.; Millam, J. M.; Iyengar, S. S.; Tomasi, J.; Barone, V.; Mennucci, B.; Cossi, M.; Scalmani, G.; Rega, N.; Petersson, G. A.; Nakatsuji, H.; Hada, M.; Ehara, M.; Toyota, K.; Fukuda, R.; Hasegawa, J.; Ishida, M.; Nakajima, T.; Honda, Y.; Kitao, O.; Nakai, H.; Klene, M.; Li, X.; Knox, J. E.; Hratchian, H. P.; Cross, J. B.; Bakken, V.; Adamo, C.; Jaramillo, J.; Gomperts, R.; Stratmann, R. E.; Yazyev, O.; Austin, A. J.; Cammi, R.; Pomelli, C.; Ochterski, J. W.; Ayala, P. Y.; Morokuma, K.; Voth, G. A.; Salvador, P.; Dannenberg, J. J.; Zakrzewski, V. G.; Dapprich, S.; Daniels, A. D.; Strain, M. C.; Farkas, O.; Malick, D. K.; Rabuck, A. D.; Raghavachari, K.; Foresman, J. B.; Ortiz, J. V.; Cui, Q.; Baboul, A. G.; Clifford, S.; Cioslowski, J.; Stefanov, B. B.; Liu, G.; Liashenko, A.; Piskorz, P.; Komaromi, I.; Martin, R. L.; Fox, D. J.; Keith, T.; Al-Laham, M. A.; Peng, C. Y.; Nanayakkara, A.; Challacombe, M.; Gill, P. M. W.; Johnson, B.; Chen, W.; Wong, M. W.; Gonzalez, C.; Pople, J. A. *Gaussian 03*, revision C.02; Gaussian, Inc.: Wallingford, CT, 2004.
(30) Becke, A. D. *Phys. Rev. A: At., Mol., Opt. Phys.* **1988**, *38*, 3098.
(31) Becke, A. D. *J. Chem. Phys.* **1993**, *98*, 5648.
(32) Lee, C.; Yang, W.; Parr, R. G. *Phys. Rev. B: Condens. Matter* **1988**, *37*, 785.
(33) Hehre, W. J.; Radom, L.; Schleyer, P. v. R.; Pople, J. A. *Ab Initio Molecular Orbital Theory*; John Wiley and Sons: New York, 1986.
(34) Andrae, D.; Haeussermann, U.; Dolg, M.; Stoll, H.; Preuss, H. *Theor. Chim. Acta* **1990**, *77*, 123.
(35) Bauernschmitt, R.; Ahlrichs, R. *Chem. Phys. Lett.* **1996**, *256*, 454.
(36) Casida, M. E.; Jamorski, C.; Casida, K. C.; Salahub, D. R. *J. Chem. Phys.* **1998**, *108*, 4439.

Scheme 1

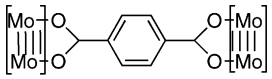

1 (R = C_6H_4)

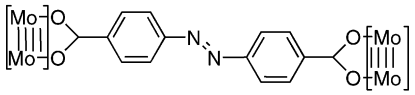

2 (R = C_6H_4-N_2-C_6H_4)

but soluble in THF. Their ^{1}H NMR spectra are as expected, and both compounds show molecular ions $\mathbf{1}^+$ and $\mathbf{2}^+$ in their MALDI mass spectra. To our knowledge, the terephthalate complex **1** has not been previously characterized. The perfluoroterephthalate analogue, however, has been reported and characterized,[39,40] and a terephthalate-bridged $[Mo_2]_2$-containing compound supported by formamidinate (ArNCHNAr, Ar = aryl) ancillary ligands has been prepared and structurally characterized by Cotton and coworkers.[41,42]

Electronic Structure Calculations. In order to aid in the interpretation of the electronic absorption spectra and the electrochemical data, vide infra, we have carried out electronic structure calculations employing DFT and TD-DFT[35−37] on the model compounds $[Mo_2(O_2CH)_3]_2(\mu\text{-}O_2CC_6H_4CO_2)$, **1′**, and $[Mo_2(O_2CH)_3]_2(\mu\text{-}O_2CC_6H_4N_2\text{-}C_6H_4CO_2)$, **2′**, where for computational simplicity, the formate ligands have been substituted for the experimental pivalate ligands. The calculations were implemented with the aid of the Gaussian 03 suite of programs using the B3LYP functional[30−32] along with the 6-31G* basis set[33] for H,C,O, and N and the SDD energy-consistent pseudopotential[34] for Mo. The geometries were fully optimized in C_{2h} symmetry, and vibrational frequency analysis found the complexes to be local minima on their respective potential energy surfaces.

The calculations on the model compound **1′** closely resembled those previously reported for the perfluoroterephthalate-bridged analogue.[38] Key features to note are that the HOMO and HOMO-1 are the out-of-phase and in-phase Mo_2 δ combinations, having b_{1g} and b_{2u} symmetry, respectively, under D_{2h} symmetry. The HOMO-1 is stabilized by back-bonding with the LUMO of the $O_2CC_6H_4CO_2$ bridge, which is a π^* orbital having carboxylate C−O antibonding character but carboxylate-C_6 ring π-bonding character. The energy separation between the HOMO and HOMO-1 is calculated to be ca. 0.2 eV, which is notably smaller than that calculated for the oxalate-bridged model complex $[(HCO_2)_3Mo_2]_2(\mu\text{-}O_2CCO_2)$.[43,44] The most intense low-energy electronic transition is calculated as the metal-to-ligand (bridge) charge transfer (MLCT) HOMO→LUMO electronic transition.

Calculations on the C_{2h}-symmetric model formate complex **2′** once again predict that the HOMO and HOMO-1 orbitals are metal-based δ combinations of b_g and a_u symmetry. These are, respectively, the out-of-phase and in-phase Mo_2 δ combinations, the latter being slightly stabilized by back-bonding to the bridge. The separation of the HOMO and HOMO-1 is calculated to be very small, ca. 0.1 eV, which indicates the Mo_2 units are only weakly electronically coupled. The HOMO-2 is calculated to be a N═N lone pair molecular orbital. Interestingly, the HOMO-3, which is 1.49 eV below the HOMO, is primarily bridge-based. This orbital also has a_u symmetry, making interaction with the δ HOMO of a_u symmetry possible. The LUMO is a bridge π^* orbital which, as in the terephthalate complex, has carboxylate C−O antibonding character and carboxylate-C_6 ring C−C π-bonding character. The HOMO−LUMO gap is calculated to be 2.4 eV.

Selected key frontier MO contour plots are given in Figure 1. The fully allowed HOMO→LUMO (MLCT) transition, calculated by TD-DFT, is 597 nm for the model compound **2′,** which compares well with that observed experimentally (λ_{max} = 606 nm, $\epsilon \approx 4 \times 10^4$ cm^{-1} M^{-1}) for complex **2** in THF. It is this absorption which gives rise to the intense blue color of **2** in solution.

Electrochemical Studies. Following the work of Taube and Richardson,[45] CV and DPV are commonly employed to evaluate the degree of electronic communication in mixed-valence complexes. The separation between the first and second oxidation potentials, $\Delta E_{1/2}$, is a measure of the relative stability of the mixed-valence complex and for a system described by eq 2. The comproportionation constant, K_c, is that defined in eq 3, where $\Delta E_{1/2}$ is in mV.

$$[Mo_2](O_2C\text{−}R\text{−}CO_2)[Mo_2] + [Mo_2](O_2C\text{−}R\text{−}CO_2)[Mo_2]^{2+} \overset{K_c}{\rightleftharpoons} 2[Mo_2](O_2C\text{−}R\text{−}CO_2)[Mo_2]^{1+} \quad (2)$$

$$K_c = \exp\frac{F\Delta E_{1/2}}{RT} \quad (3)$$

As we and others have noted, although electrochemical studies are convenient, the interpretation of the magnitude of K_c with respect to classification on the Robin and Day scheme can be tenuous at best.[46−48] K_c is a thermodynamic parameter and is dependent on the solvent and the counteranion for any given system. Moreover, neither CV nor DPV inform one of whether the metal centers or the bridge are

(37) Stratman, R. E.; Scuseria, G. E.; Frisch, M. J. *J. Chem. Phys.* **1998**, *109*, 8218.
(38) Dennington, R. K. T., II; Millam, J.; Eppinnett, K.; Hovell, W. L.; Gilliland, R. *GaussView, Version 3.09*; Semichem, Inc.: Shawnee Mission, KS, 2003.
(39) Bursten, B. E.; Chisholm, M. H.; Clark, R. J. H.; Firth, S.; Hadad, C. M.; Macintosh, A. M.; Wilson, P. J.; Woodward, P. M.; Zaleski, J. M. *J. Am. Chem. Soc.* **2002**, *124*, 3050.
(40) Cayton, R. H.; Chisholm, M. H.; Huffman, J. C.; Lobkovsky, E. B. *J. Am. Chem. Soc.* **1991**, *113*, 8709.
(41) Cotton, F. A.; Donahue, J. P.; Lin, C.; Murillo, C. A. *Inorg. Chem.* **2001**, *40*, 1234.
(42) Cotton, F. A.; Lin, C.; Murillo, C. A. *J. Chem. Soc., Dalton Trans.* **1998**, 3151.
(43) Bursten, B. E.; Chisholm, M. H.; Clark, R. J. H.; Firth, S.; Hadad, C. M.; Wilson, P. J.; Woodward, P. M.; Zaleski, J. M. *J. Am. Chem. Soc.* **2002**, *124*, 12244.
(44) Chisholm, M. H.; D'Acchioli, J. S.; Hadad, C. M.; Patmore, N. J. *Dalton Trans.* **2005**, 1852.
(45) Richardson, D. E.; Taube, H. *Inorg. Chem.* **1981**, *20*, 1278.

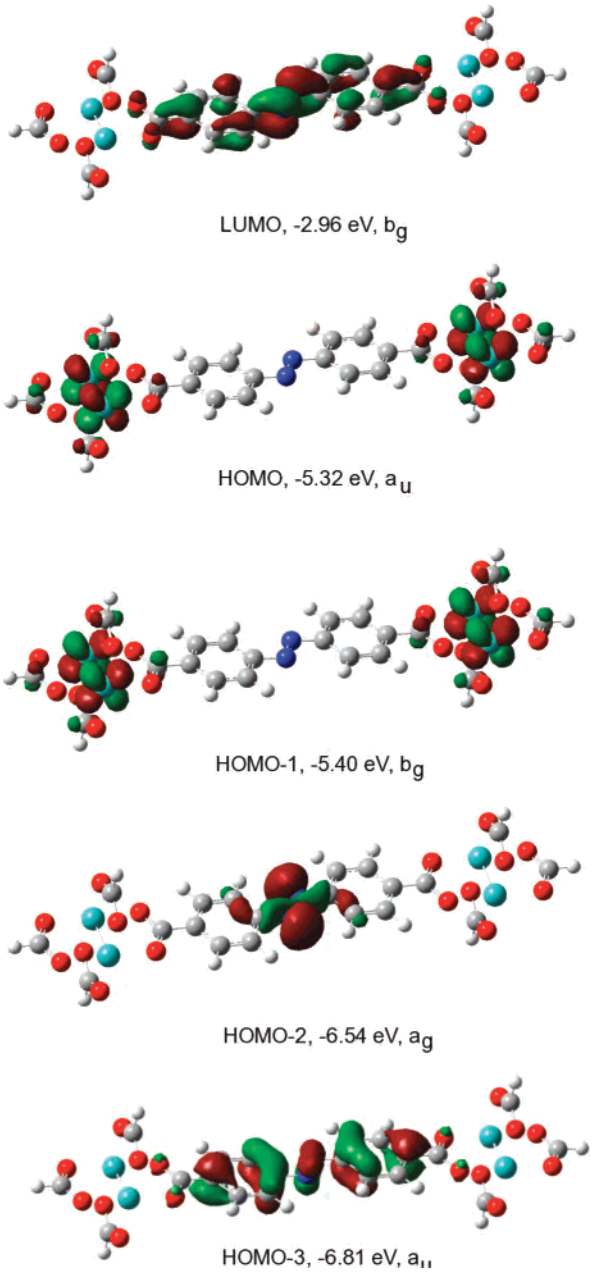

Figure 1. Selected frontier molecular orbital plots for $[Mo_2(O_2CH)_3]_2(\mu\text{-}O_2CC_6H_4N_2C_6H_4CO_2)$. Orbital plots were generated using GaussView, with an isosurface value of 0.02.

being oxidized or reduced. However, if it is known that the metal centers are being oxidized (or reduced), then a small value of K_c (<100) can reasonably be taken as indicative of weak electronic coupling; a large value can be taken as an indication of strong coupling (Class II or III on the Robin and Day scheme). However, the value of K_c should not be employed in isolation to uniquely distinguish between strongly coupled and fully delocalized systems.

Electrochemical studies on **1** and **2** were carried out in a 0.1 M $TBAPF_6$/THF (TBA = $[^nBuN]_4$) solution. Both complexes exhibited a single oxidation wave at ca. −0.1 V relative to the $Cp_2Fe^{0/+}$ couple, which was quite broad for **1**. For both complexes this wave is assigned to two overlapping one-electron oxidation processes. However, when 0.05 M $TBABArF_{24}$ [$BArF_{24}$ = 3,5-$(CF_3)_2C_6H_3$] electrolyte solutions in THF were employed, two successive oxidation waves were observed at −0.02 and −0.168 V (vs $Cp_2Fe^{+/0}$) for the terephthalate complex **1**. This gives $\Delta E_{1/2}$ = 148 mV and K_c (from eq 3) = 324. For complex **2** only one two-electron process was observed, even when employing the $TBABArF_{24}$ electrolyte.

The above example highlights the effect of employing the large, weakly coordinating $BArF_{24}^-$ counteranion on maximizing $\Delta E_{1/2}$ values for successive oxidation processes, as has been pointed out by Geiger and co-workers.[46] The electrochemical results indicate that the ions $\mathbf{1}^+$ and $\mathbf{2}^+$ are to be considered very weakly coupled at best, and indeed, $\mathbf{2}^+$ has a K_c close to the statistical minimum of 4 and is valence-trapped (Class I on the Robin and Day classification scheme).

What governs the communication between metal centers? The answer is a delicate balance of factors. Cotton and co-workers have shown that in Mo_2 quadruply linked compounds of the type $[Mo_2]_2(\mu\text{-}O_2C{-}(CH{=}CH)_n{-}CO_2)$ the electronic coupling rapidly dropped off with increasing n (n = 0−4).[14] As we have shown, the oxalate-bridged radical cation $[(^tBuCO_2)_3Mo_2]_2(\mu\text{-}O_2CCO_2)^+$ with a Mo_2-to-Mo_2 separation of ∼7 Å shows fully delocalized properties.[49] The $[(^tBuCO_2)_3Mo_2]_2(\mu\text{-}O_2CC_6F_4CO_2)^+$ ion has a Mo_2-to-Mo_2 separation of ∼11 Å and displays an EPR spectrum consistent with a valence-trapped Mo_2^{5+} core having $A_o \approx$ 28 G for coupling to ^{95}Mo and ^{97}Mo (I = 5/2). Given the extent of electronic coupling, it is thus perhaps not surprising, but rather to be expected, that the electronic coupling in $\mathbf{2}^+$ is negligible given that it is small in $\mathbf{1}^+$ for Mo_2-to-Mo_2 distances of ca. 19 vs ca. 11 Å for **2** and **1**, respectively. What, then, causes the $[(trpy)(bpy)Ru]_2(\mu\text{-}NCNC_6H_4NCN)^{3+}$ complex to be more weakly coupled than the $[(trpy)(bpy)Ru]_2(\mu\text{-}NCNC_6H_4N_2C_6H_4NCN)^{3+}$ ion, which is made evident by K_c values of 2.7×10^7 and 1.3×10^{13}, respectively?[20,21]

The Azobisphenylcyanamido (adpc^{2-}) Bridge. By employing DFT and TD-DFT with the Gaussian 03 suite of programs (vide supra), we start by examining the structure of the ligand bridge dianion, $adpc^{2-}$. The calculated gas-phase structure was obtained by geometry optimization of the dianion under C_{2h} symmetry. This molecular ion can be considered as the sum of three rigid fragments −NCN− = A, $-C_6H_4-$ = B, and −NN− = C arranged in the symmetrical manner A−B−C−B−A. The utility of employing this view is that the resultant molecular orbitals can be traced to their origins in the individual units of A, B, and C. At the DFT level, the HOMO and HOMO-1 are π-based MOs having −NCN− nitrogen lone-pair character together with contribution from the phenyl and azo systems. In the

(46) Barriere, F.; Camire, N.; Geiger, W. E.; Mueller-Westerhoff, U. T.; Sanders, R. *J. Am. Chem. Soc.* **2002**, *124*, 7262.
(47) Chisholm, M. H.; Clark, R. J. H.; Gallucci, J. C.; Hadad, C. M.; Patmore, N. J. *J. Am. Chem. Soc.* **2004**, *126*, 8303.
(48) D'Alessandro, D. M.; Keene, F. R. *Dalton Trans.* **2004**, 3950.
(49) Chisholm, M. H.; Pate, B. D.; Wilson, P. J.; Zaleski, J. M. *Chem. Commun.* **2002**, 1084.
(50) Sondaz, E.; Gourdon, A.; Launay, J.-P.; Bonvoisin, J. *Inorg. Chim. Acta* **2001**, *316*, 79.

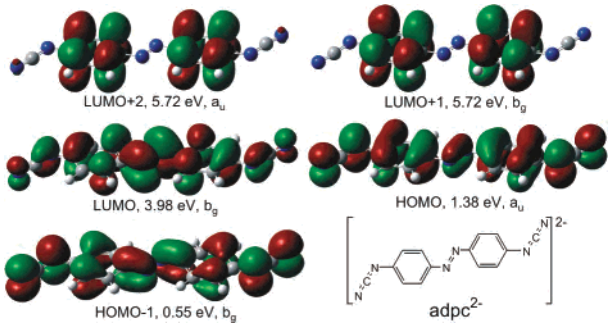

Figure 2. Selected frontier molecular orbital plots for adpc^{2-}. Orbital plots were generated using GaussView, with an isosurface value of 0.02.

HOMO, the azo N═N contribution is bonding, and in the HOMO-1, it is antibonding. The phenyl ring π-contribution to each of these MOs can be considered to be derived from the e_1 π-set of benzene and in the HOMO-1, this leads to azo nitrogen-to-ring carbon π-bonding (see Figure 2). The calculated difference in energy between these occupied frontier orbitals is 0.83 eV. Below these come in-plane nitrogen lone pairs, with the HOMO-2 being centered on the azo nitrogens and the HOMO-3 on the −NCN groups. They are separated from the HOMO by 1.49 and 1.94 eV, respectively. These are the only significant occupied π-type bridge MOs that will interact with the filled Ru t_{2g}^6-type orbitals (metal d_π), and clearly the dominant interactions will be with the HOMO and HOMO-1 since the HOMO-3 is stabilized by roughly 2 eV and the HOMO-2 is centered on the azo unit.

The LUMO, LUMO+1, and LUMO+2 of adpc^{2-} are also shown in Figure 2. The LUMO is similar to the HOMO in being composed of contributions from all three fragments A + B + C and is again −NCN− π-lone pair in character and azo-N−N antibonding. The aromatic π component has two nodal planes (perpendicular to the C_6 plane), and as such, is derived from the e_2 benzene π-set, and the cyanamide N-to-ring C_6-carbon interaction is bonding. A visual inspection of the orbital isosurfaces shows the contribution from the terminal nitrogens is less than that in the HOMO and HOMO-1. The LUMO+1 is also a very simple orbital in its makeup, having only significant contributions from the C_6 ring carbon π atomic orbitals, and may be considered to be derived from the e_2 π-set orbitals of benzene. The LUMO+2 is similarly C_6 centered, and the only significant difference between the LUMO+1 and LUMO+2 is that the former has a center of inversion about the N−N centroid and the latter does not. The calculated HOMO−LUMO energy gap is 2.60 eV, and the energies of the LUMO+1 and LUMO+2 are similar, but both higher-lying virtual orbitals are calculated to be greater than 1.7 eV above the LUMO. Thus, by symmetry, overlap, and energy considerations, only the HOMO, HOMO-1, and LUMO of the adpc^{2-} bridge will interact significantly with the Ru t_{2g}^6 centers.

At this point, it is worth noting that DFT-based HOMO and LUMO orbitals are pictorially equivalent in this study to that reported earlier using Hartree−Fock (HF) orbitals,[20] and the earlier calculation (HF/6-311G**) employing the SPARTAN suite of programs (version 5.01) yielded a much

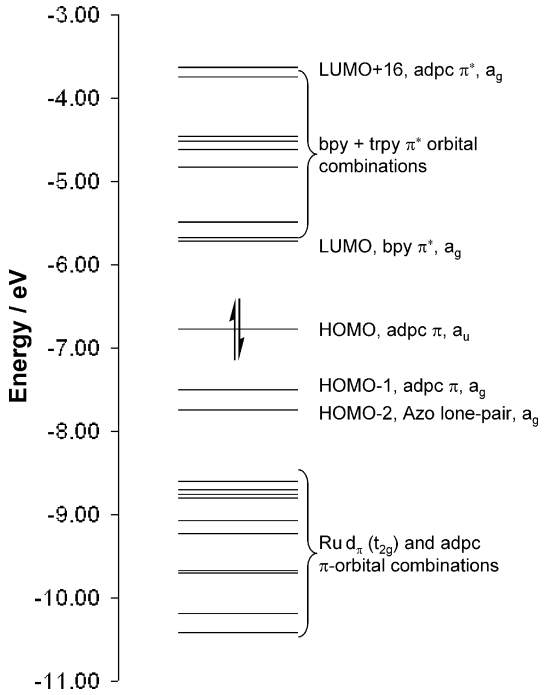

Figure 3. Frontier molecular orbital diagram calculated for [(trpy)(bpy)-Ru]$_2$(μ-adpc)$^{2+}$.

smaller HOMO−LUMO gap of 1.07 eV. We also note that the calculated electronic absorption spectra for the adpc^{2-} anion, obtained by TD-DFT calculations in this study, has the lowest-energy $\pi \rightarrow \pi^*$ absorption at 473 nm (2.62 eV). This absorption is dominated by the fully allowed HOMO→LUMO configuration. The calculated TD-DFT absorption compares quite favorably with the reported solution λ_{max} at 523 nm (2.37 eV) for adpc^{2-} in DMF solutions.[12] However, on the basis of a 1.07 eV HOMO−LUMO gap at the HF level, we might roughly expect a lowest-energy HOMO→LUMO absorption at around 1160 nm.

The Diruthenium adpc Ion. The calculations on [(trpy)-(bpy)Ru]$_2$(μ-adpc)$^{2+}$ (α) were carried out using a single-point calculation based on the atomic coordinates taken from the structure obtained by a single-crystal X-ray study. This molecular ion has a crystallographically imposed center of inversion which endears itself to a comparison with the electronic structure of the adpc^{2-} ion just described.

A molecular orbital energy level diagram calculated for [(trpy)(bpy)Ru]$_2$(μ-adpc)$^{2+}$ is given in Figure 3, and selected occupied frontier molecular orbital isosurface plots are shown in Figure 4. The HOMO can be seen to be predominantly the bridge-based HOMO of the adpc^{2-} ligand, with a small contribution from a Ru t_{2g}-type orbital. The metal d_π−bridge π interaction is antibonding, as expected for a filled−filled interaction. The HOMO-1 can once again be seen to be bridge-based and is derived from the HOMO-1 of the free ligand bridge, which is N−N π-antibonding, as shown in Figure 2. There is again a small amount of Ru d_π-antibonding character, but this is slightly more than in the HOMO because it is closer in energy to the filled Ru t_{2g} orbitals. The calculated HOMO-to-HOMO-1 gap is 0.73 eV, which is only slightly smaller than 0.83 eV calculated for the free ligand bridge. The HOMO-2 is an in-plane azo nitrogen lone pair

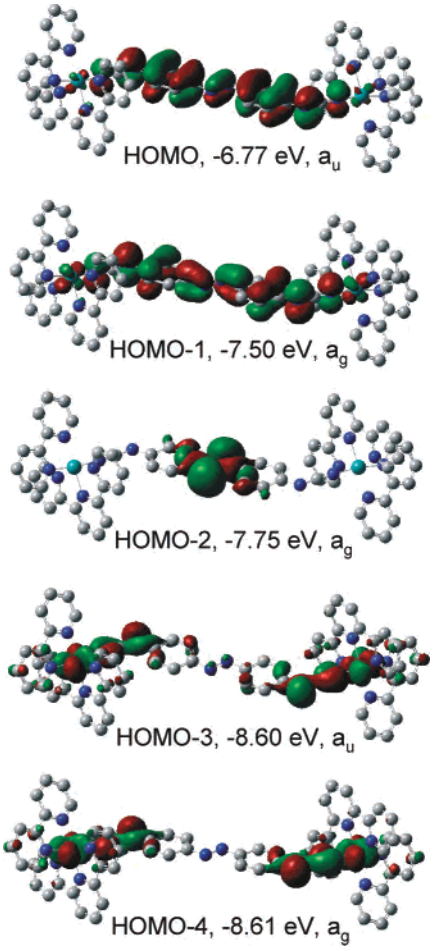

Figure 4. Selected occupied frontier molecular orbital plots for [(trpy)(bpy)Ru]$_2$(μ-adpc)$^{2+}$. Orbital plots were generated using GaussView, with an isosurface value of 0.02. Hydrogen atoms have been omitted for clarity.

combination and is 0.98 eV below the HOMO. Below this comes a degenerate pair of orbitals that are in-plane cyanamide nitrogen p_π lone pairs which are bonding to metal in-plane t_{2g}-type orbitals. These are calculated to be 1.83 eV below the HOMO, and these orbitals are the *first* to be seen that have a *significant* amount of metal characters. The HOMO-5 is a ligand bridge π MO having some small contribution from a Ru t_{2g} combination, and the HOMO-6 is a ligand bridge C_6-based π MO. This is at 1.99 eV below the HOMO. Orbital plots of other frontier molecular orbitals having significant Ru $d_\pi-t_{2g}$ and bridge$-\pi$ character are given in the Supporting Information.

What is perhaps surprising is the relatively insignificant contribution of the Ru t_{2g} orbitals to this frontier manifold. However, whereas the cyanamide ligands can be viewed as π-donors, the other ancillary ligands present, namely bpy and trpy, are powerful π-acceptors, and it is this effect that is stabilizing the t_{2g} set. Evidence of this can be seen from an examination of the lowest-energy unoccupied MOs. The LUMO is 1.06 eV higher in energy than the HOMO and is based on the bpy π^* ancillary ligand. The bpy/terpy π^*-orbital combinations continue until the LUMO+16, which is the first unoccupied orbital in which we observe a significant contribution from the bridge π^* system (see Figure 5).

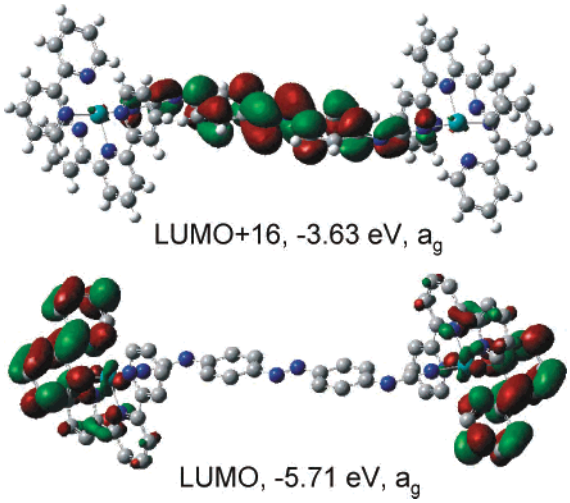

Figure 5. Selected unoccupied frontier molecular orbital plots for [(trpy)(bpy)Ru]$_2$(μ-adpc)$^{2+}$. Orbital plots were generated using GaussView, with an isosurface value of 0.02. Hydrogen atoms have been omitted for clarity.

From the calculated results, we can surmise that the metal t_{2g}^6-based electrons are preferentially stabilized by the bpy/trpy ligands and that the bridge-based π MOs are destabilized by their interaction with the t_{2g}^6 electrons such that they are the highest occupied MOs. From an initial interpretation, the computational results cast doubt on the notion that oxidation of the Ru(II)$-$adpc$-$Ru(II) complex will result in oxidation of ruthenium. Indeed, the data suggest that oxidation will involve removal of an electron from a bridge-based molecular π orbital. Inspection of the HOMO and HOMO-1 reveals very little metal d_π character; these orbitals are separated by 0.73 eV. A more comprehensive computational study is currently underway.

As noted in the introduction, we can think of the bridge as being assembled from components A$-$B$-$C$-$B$-$A where A is $-$NCN$-$, B is $-C_6H_4-$, and C is $-$N$=$N$-$. In the HOMO, the AB π system is combined in an antibonding manner with the azo N_2 π-bonding orbital, while in the HOMO-1, the AB π system is combined with the N_2 π^* MO in a bonding manner. In each of these orbitals, the majority of the π-electron density is on the C_6 rings. It is thus plausible to think of oxidation as generating a fully delocalized organic radical and that the low-energy IVCT band arises from the HOMO-1-to-HOMO electronic transition. Indeed, as a very crude approximation, the calculated separation between the HOMO and HOMO-1 in [(trpy)(bpy)Ru]$_2$(μ-adpc)$^{2+}$ of 0.73 eV (5887 cm^{-1}) compares favorably with the observed IVCT absorption for [(trpy)(bpy)Ru]$_2$(μ-adpc)$^{3+}$ in acetonitrile at 5556 cm^{-1}.[12] The N_2 unit serves to couple the two AB π systems which, in turn, are stabilized toward oxidation by interaction with the Ru t_{2g} d_π electrons. However, the Ru t_{2g}^6 π electrons are, for the most part, stabilized by backbonding to the trpy and bpy π^* orbitals which are much lower in energy than the π^* orbitals of the NCN groups of the bridge.

Concluding Remarks

In the present work, we find that the terephthalate bridge is more effective in electronic coupling between Mo_2

quadruply bonded centers than is the longer 4,4′-azodibenzoate. In comparing the 4,4′-azodibenzoate bridge with the 4,4′-azodiphenylcyanamide bridge, we note that the former acts primarily through electron transfer via the π^* orbitals of the bridge, while the cyanamide bridge is more suited to coupling by a hole-transfer mechanism. The calculations on the adpc ion, limited as they are to a single-point calculation for a gas-phase ion and pertaining to the $Ru^{II}\cdots Ru^{II}$ species, do cast reasonable doubt concerning the site of oxidation. The electrochemical data and the appearance of the low-energy charge resonance band in the near-IR spectrum of the mixed-valence compound could well be accounted for by oxidation of the bridge. We note, for example, that other dinuclear ruthenium (II,II) complexes bearing π-acceptor ligands have been unequivocally shown to undergo oxidation of the bridge and not the ruthenium.[51−53] Consequently, we hope that this work will stimulate further experimental studies on this remarkable ion. We note, for example, that an EPR study on the product of single-electron oxidation should be useful in discerning between a Ru- or organic-based radical.[50]

Finally, let us consider what is implied for a Class III ion of the form $[M-A-B-A-M]^{n(\pm)}$ and $[M-A-B-C-B-A-M]^{n(\pm)}$ where the charge is fully delocalized over both centers M. In a super exchange mechanism for a through-bond process, the π orbitals of the bridge must couple with the metal d_π orbitals in a coherent manner as in any extended π chain. The coupling of the two metal centers will therefore decrease with increasing chain length. If A and B remain the same, then no matter what the nature of C, the longer chain will not be coupled as strongly as the shorter chain. If the two centers M are coupled in an incoherent manner, then electron transfer by an electron or hole-hopping mechanism may be facilitated by the introduction of some group C along a longer-distance pathway. Such a mechanism may facilitate charge transfer through a polymer or a strand of DNA but does not constitute the mechanism of electronic coupling in mixed-valence ions having Class III characteristics. It is therefore not conceivable to us that, in a coherent superexchange mechanism, electronic coupling across a $[NCN-C_6H_4-N_2-C_6H_4-NCN]^{2-}$ (A−B−C−B−A) bridge should be greater than for $[NCN-C_6H_4-NCN]^{2-}$ (A−B−A) bridge.

Acknowledgment. The authors thank the National Science Foundation for financial support and gratefully acknowledge the Ohio Supercomputer Center for generous allocations of computing time and Professor F. A. Cotton for stimulating discussions. J.S.D. gratefully acknowledges Dr. Kari Greenchurch and Nan Kleinholz for assistance with obtaining mass spectra. J.S.D. especially acknowledges Dr. Matthew Byrnes for his patience, guidance, and support.

Supporting Information Available: Geometry-optimized coordinates of $[(HCO_2)_3Mo_2]_2(\mu\text{-adb})$ and $[(HCO_2)_3Mo_2]_2(\mu\text{-}O_2CC_6H_4CO_2)$; atomic coordinates calculated for $adpc^{2-}$; and selected occupied frontier molecular orbital diagrams for $[(trpy)(bpy)Ru]_2(\mu\text{-adpc})^{2+}$. This material is available free of charge via the Internet at http://pubs.acs.org.

IC060956W

(51) Meacham, A. P.; Druce, K. L.; Bell, Z. R.; Ward, M. D.; Keister, J. B.; Lever, A. P. B. *Inorg. Chem.* **2003**, *42*, 7887.
(52) Maurer, J.; Winter, R. F.; Sarker, B.; Fiedler, J.; Zális, S. *Chem. Commun.* **2004**, 1900.
(53) Maurer, J.; Sarker, B.; Schwederski, B.; Kaim, W.; Winter, R. F.; Zális, S. *Organometallics* **2006**, *25*, 3701.